The Influence of Multiple Scattering on Lidar Returns by Cirrus Clouds and an Effective Inversion Algorithm for the Extinction Coefficient

G. H. RUPPERSBERG, M. KERSCHER[1], M. NOORMOHAMMADIAN[2], U. G. OPPEL[2] AND W. RENGER

Institut für Physik der Atmosphäre, Deutsche Forschungsanstalt für Luft- und Raumfahrt (DLR), 82230 Oberpfaffenhofen, Germany
[1] Sektion Physik, Ludwig-Maximilians-Universität München, Theresienstraße 37, 80333 München
[2] Mathematisches Institut, Ludwig-Maximilians-Universität München, Theresienstraße 39, 80333 München

Abstract

A new effective inversion method for lidar return signals is presented. For the derivation of this inversion formula the multiple scattering term is approximated by the sum of the single and double scattering part of the lidar return signal. This inversion algorithm was tested against simulated lidar profiles for different cloud types, including all scattering orders by making use of variance reduction Monte Carlo methods.

The results show good agreement for the situations of typical ground-based lidar measurements in cirrus clouds. The new algorithm is stable concerning the assumptions made on the type of the phase function in the unknown cloud. Furthermore the simulations demonstrate that the double scattering contribution is increasing within the cloud with increasing optical depth. At the upper boundary of the cloud it is approaching the product of optical depth times the single scattering contribution. Beyond the cloud with increasing distance, this contribution is slowly decreasing.

1 Introduction

Multiple scattering in the atmosphere is less important when using lasers for remote sensing applications in contrast to the transfer of natural radiation in the atmosphere. This is due to the small divergence of the pulsed laser beam and the narrow field of view of the receiving telescopes. Still, multiple scattering should not be neglected especially for high optical depths (e.g. Eloranta, 1972; Platt, 1973; Bissonnette et al., 1995). As an example, Blaettner et al. (1974), p. 55, found that 50 % of the lidar signal was produced by multiple scattering at optical depths of 2. Therefore multiple scattering effects are essential in the case of lidar slant visibility measurements (Werner et al., 1992), but the multiply scattered component of the lidar return signal has been widely considered as negligible for an optical depth of less than some 0.1. Consequently, the standard lidar inversion methods for atmospheric haze and op-

tically thin clouds assume single scattering only (e.g. Klett, 1980; Klett, 1981; Klett, 1985; Schmitz-Peiffer and Renger, 1991).

Despite of this, during the International Cirrus Experiment (ICE) with the ALEX lidar (Moerl et al., 1981) it was shown that neglecting multiple scattering leads to meaningless results even for small optical depths of some 0.01 (e.g. Ruppersberg and Renger, 1990; Gratzki, 1991; Kaestner et al., 1993). Gratzki (1991) treats multiple scattering with an empirically extended version of the Klett algorithm (Carnuth and Reiter, 1986). In this approach the resulting extinction coefficient which tends to be too high, is corrected by application of a parametric factor (e.g. Eloranta, 1972; Platt, 1973). Ruppersberg and Renger (Kaestner et al., 1993) introduced a multiple scattering term in a mathematically correct way. Here the multiple scattering term of the lidar equation is approximated by the second order scattering. It should

be mentioned that the often not well known lidar ratio (see Eq. (2.8)) does not touch the results for the double scattering contribution. Therefore this question will not be discussed throughout this paper. Related problems can be found in a recent paper by Wandinger (1996).

The restriction to double scattering is supported by studies made by, e.g. Eloranta, 1972; Weinman, 1976; van de Hulst, 1980. Phase functions of ice crystals in cirrus clouds show even steeper forward scattering peaks compared to those of water droplet clouds (e.g. Wendling, 1979; Hess and Wiegner, 1991 and 1994; Strauss and Wendling, 1992; Strauss, 1994). The major part of the radiation which is forward scattered by cirrus particles remains within the telescope field of view (FOV) for long distances. At maximum the value of this second order component is reaching the value of the optical thickness of the cloud. The contribution from double scattering may also affect stratospheric lidar measurements if an even optically thin tropospheric cloud was penetrated, which might not be detected due to the common blocking of short distance signals.

Extreme forward scattering in ice clouds is quite common and not exceptional, which is readily observed when, e.g., the sun is still apparent behind a cirrus: the contours are blurred. With increasing optical depth of the cirrus, the sun disc disappears before its aureole (see also van de Hulst (1980) p. 660f.). Also, contours seen through snow showers seem blurred. This is opposite to liquid water clouds or fog, which show a pale but sharp sun disc, appearing or disappearing with sharp boundaries.

The multiple scattering term of the lidar equation used in our inversion is calculated making two assumptions: first, it is sufficient to take into account only second order scattering, and second, the phase function is sufficiently represented by its value at the scattering angle zero and it's steepness following from the Babinet theorem. This study examines the validity of these assumptions by comparing the approximation with unbiased and variance controlled estimates based on the exact stochastic model for multiple scattering (Noormohammadian, 1996).

2   Lidar Equation Including Multiple Scattering

Consider a lidar system which emits P_i photons in a short pulse at time $t = 0$. Propagating through the atmosphere, a certain amount of them is scattered and absorbed by molecules, aerosol particles, and cloud particles. At time t, corresponding to a range $r = ct/2$ (c denotes the speed of light), a small number of photons

$$\Delta P(r) = \Delta P^{(1)}(r) + \Delta P^{(m)}(r) \qquad (2.1)$$

is received by the lidar system. The component $\Delta P^{(1)}(r)$ is the number of singly scattered photons in a range interval ("sampling interval") $\Delta r = c\Delta t/2$, whereas the other component $\Delta P^{(m)}(r)$ is the number of multiply scattered photons.

With the definition of the multiple scattering factor

$$Q_{ms}(r) = \frac{\Delta P^{(m)}(r)}{\Delta P^{(1)}(r)}, \qquad (2.2)$$

we get

$$\Delta P(r) = \Delta P^{(1)}(r)\,(1 + Q_{ms}(r)). \qquad (2.3)$$

The single scattering component is calculated from the classical single scattering lidar equation.

Then Equation (2.3) may be written as

$$\Delta P(r) = P_i\,\Delta r\,A\,\frac{\beta(r)\tau^2(r)}{r^2}\,(1 + Q_{ms}(r)). \qquad (2.4)$$

A is the effective receiver area. The backscatter coefficient $\beta(r)$ $(\equiv \beta(\pi,r))$ is the value of the scattering function in the sampling volume at position r for scattering angle of $\vartheta = \pi$; $\tau(r)$ is the regular (or direct) transmittance of the atmosphere between the lidar system and the sampling interval at range r. The regular transmittance obeys the Bouguer-Lambert law

$$\tau(r) = \exp\left(-\int_0^r \sigma_e(r')\,dr'\right), \qquad (2.5)$$

with the range-dependent extinction coefficient $\sigma_e(r')$ at distance r'.

Eq. (2.4) is valid for systems whose receiver FOV is larger than the laser beam divergence, for short pulse durations compared to the sampling intervals, and for ranges $r \geq r_{min}$, with r_{min} being the minimum range where the laser beam has completely entered the FOV of the receiver telescope.

Let η be the total efficiency of the receiving system that is the number of counts per received photon. Then the range-corrected receiver counts per sample interval are

$$\Delta D(r) = \eta \, \Delta P(r) \, \frac{r^2}{r_0^2}. \tag{2.6}$$

r_0 is a fixed reference distance, e.g. 1000 m. Height and contours of clouds are immediately apparent in the range-corrected counts, whereas the physical quantities (backscatter coefficients, optical depths, etc.) need to be retrieved by an inversion of Eq. (2.4). Summarizing the constants to a system factor:

$$K = \frac{r_0^2}{\eta \, P_i \, A}, \tag{2.7}$$

we obtain from Eqs. (2.4), (2.6) and (2.7)

$$\sigma_e(r)\Delta r = K(\sigma_e/\beta)(r)\frac{\Delta D(r)}{\tau^2(r)(1 + Q_{ms}(r))}. \tag{2.8}$$

In the troposphere both, β and σ_e, vary by more than 6 orders of magnitude. The so-called lidar ratio (σ_e/β) varies by less than 2 magnitudes. For pure molecular (Rayleigh) scattering the lidar ratio is 8.38. For other cases average values are 14 for cirrus, 20 for water clouds, 23 (50) for fresh (aged) volcanic dust and 30 for maritime aerosol, 48 for tropospheric, 50 for rural, and 67 for urban aerosol (Pinnick et al., 1983; Dubinsky et al., 1985; Jursa, 1985). The lidar ratio can be determined using additional information via the IR-emission (Platt, 1973), the shadow technique (Kaestner et al., 1993), Raman or high spectral resolution lidars (Ansmann et al., 1992; Wandinger, 1996). We assume the factor $K(\sigma_e/\beta)$ to be known. This work is dealing with the effect of multiple scattering which is independent from the lidar ratio. For the calculation the common separation into a Mie- and a Rayleigh-part has to be performed. With an estimate of $Q_{ms}(r)$ as given later in Eq. (3.13), Eq. (2.8) can be solved iteratively for the range step

$$r_i = (i - \frac{1}{2}) \, \Delta r \quad \text{with} \quad i = 1, \dots, n \tag{2.9}$$

where n denotes the number of range bins to be analysed. With $\tau(r_1) = 1$ the regular transmittance at each range step $r_{i+1} = r_i + \Delta r$ is estimated from Eq. (2.5) with

$$\tau(r_{i+1}) \approx \tau(r_i)\exp\left(-\sigma_e(r_i)\Delta r\right). \tag{2.10}$$

3 An Effective Algorithm for the Multiple Scattering Contribution Q_{ms}

For the calculation of lidar signals with receiver FOV angles α of less than ± 5 mrad and for clouds with an optical thickness of some 0.1, it is sufficient, as we will show in Section 5, to neglect multiple scattering orders higher than 2. We therefore define the double scattering factor analogue to the multiple scattering factor of Eq. (2.2)

$$Q_{ms}^{(2)}(r) = \frac{\Delta P^{(2)}(r)}{\Delta P^{(1)}(r)}, \tag{3.1}$$

and approximate in Eq. (2.8)

$$Q_{ms}(r) \approx Q_{ms}^{(2)}(r). \tag{3.2}$$

Double scattering contributes to the lidar return signal from the distance r with two different portions of photons: The first portion is the amount of primarily forward scattered photons at distances $r_p \leq r$ which are secondarily backward scattered from the volume element $\Delta r \, FOV(r)$ (with the field of view $FOV(r) = \pi\alpha^2 r^2$ at distance r). The second portion is the amount of primarily backward scattered photons at the distance r which are in a second step forward scattered from the volume elements $\Delta r \, FOV(r_s)$ at distances $r_s \leq r$.

Considering usual lidar devices with FOV half aperture angles of $\alpha \leq 5$ mrad, the second portion of the doubly scattered photons is equal to the first, and customary radiation flux calculations result in

$$Q_{ms}^{(2)}(r) \approx 2 \cdot \frac{2\pi}{\beta'(\pi,r)} \int_0^r \int_0^{\vartheta_{pm}} \sigma_s(r_p) \tag{3.3}$$
$$\beta'(\vartheta_p, r_p) \, \beta'(\vartheta_s, r) \, \sin(\vartheta_p) \, d\vartheta_p \, dr_p$$

where $\sigma_s(r_p)$ is the scattering coefficient at position r_p, and $\beta'(\vartheta, r)$ is the phase function at distance r (with integral over ϑ equal to 1) defined by

$$\beta'(\vartheta, r) = \frac{\beta(\vartheta, r)}{\sigma_s(r)}. \tag{3.4}$$

Furthermore, ϑ_p is the angle of primary scattering and ϑ_s is the angle of secondary scattering. Because of the geometry of double scattering ϑ_s and the upper limit of ϑ_p, ϑ_{pm}, follow from the equations

$$\vartheta_s = \pi - \vartheta_p + \arctan\left(\frac{r - r_p}{r}\tan\vartheta_p\right), \quad (3.5)$$

$$\vartheta_{pm} = \arctan\left(\frac{r}{r - r_p}\tan\alpha\right). \quad (3.6)$$

The scattering coefficient $\sigma_s(r_p)$ is

$$\sigma_s(r_p) = \sigma_e(r_p)\left(1 - \frac{\sigma_a}{\sigma_e}(r_p)\right). \quad (3.7)$$

The absorption coefficient σ_a is negligible compared with σ_e and is no longer taken into account.

The conditions for the Eqs. (3.2) and (3.3), as well as the more complicated equations without the *FOV* restrictions, have been extensively verified with the exact stochastic model (see Section 4). Still, for mass data evaluation, even Eq. (3.3) is too time consuming. Therefore we assume

$$\beta'(\vartheta_s, r) \approx \beta'(\pi, r), \quad (3.8)$$

and that the phase function within the angular range of forward scattering $\vartheta_p = (0 \pm \text{some mrad})$ may be approximated by the exponential law depending on the wavelength λ (see Figure 1 and Figure 2)

$$\beta'(\vartheta_p, r_p) \approx \beta'_\lambda(0, r_p)\exp\left(-\frac{\vartheta_p}{\vartheta_w(\lambda, r_p)}\right). \quad (3.9)$$

Better fits for the shape of the phase function e.g. a Gaussian approximation are possible. But this approach allows for an analytical integration of Eq. (3.3) making the inversion comfortably fast. Within cirrus clouds the diffraction lobe dominates forward scattering into the angular range that mainly contributes to the integral in Eq. (3.3). The Babinet theorem (e.g. Muetze et al., 1961) states that the diffraction lobe produces 50 % of the extinction coefficient σ_e, and its width is inversely proportional to the wavelength λ. For the $1/e$-width $\vartheta_w(\lambda, r_p)$ in Eq. (3.9) at laser wavelength λ we get

$$\vartheta_w(\lambda, r_p) \approx \frac{1}{2\sqrt{\pi\,\beta'_{\lambda_0}(0, r_p)}}\frac{\lambda}{\lambda_0}. \quad (3.10)$$

This equation delivers the $1/e$-width at any wavelength λ from the values $\beta'_{\lambda_0}(0, r_p)$ of published phase functions for the wavelength λ_0 (e.g. Hess and Wiegner, 1991 and 1994; Strauss and Wendling, 1992; Strauss, 1994). From Table 2 one may verify this dependency. Examples are discussed in Section 5.

Using Eqs. (3.7), (3.8), and (3.9), Eq. (3.3) now may be integrated analytically over ϑ_p, and it follows the approximated double scattering factor $Q_{ms}^{(2)}(r) \approx Q_{ms}^{(2a)}(r)$ with

$$Q_{ms}^{(2a)}(r) \quad (3.11)$$

$$= \int_0^r \sigma_e(r_p)\left[1 - \left(1 + \frac{r}{r - r_p}\frac{\alpha}{\vartheta_w(\lambda, r_p)}\right)\right.$$

$$\left.\exp\left(-\frac{r}{r - r_p}\frac{\alpha}{\vartheta_w(\lambda, r_p)}\right)\right]\,dr_p.$$

The result is highly dependent on the ratio FOV to width of the diffraction lobe, which was pointed out by Eloranta (1972). The term in the square brackets converges to 1 for $r_p \to r$, that is for the last sample interval of this integral, and therefore, Eq. (3.11) results in

$$Q_{ms}^{(2a)}(r_p = r) \approx \Delta r\,\sigma_e(r_p). \quad (3.12)$$

The radiation flux scattered into the diffraction lobe of the ice crystals of this sample interval remains completely within the lidar receiver *FOV*, thus appearing completely as contribution to the illumination which causes backscattering.

The same applies for larger range differences $(r - r_1)$, if the diffraction lobe is narrow enough. Then practically all scattered radiation remains in the *FOV*, and the double scattering factor is maximal, with a value equal to the optical thickness of the cloud in which the primary scattering occurred.

Concerning "similar" cloud stratifications, whose extinction coefficients differ only by a height-independent factor, Eq. (3.11) states that $Q_{ms}^{(2)}(r)$ is proportional to the extinction coefficient at any position within the clouds and, hence, to the optical depth of the clouds.

The multiple scattering factor is calculated for every range step r_i combining Eqs. (3.11) and (3.12). We get $Q_{ms}^{(2a)}(r_1) = 0$ and

$$Q_{ms}^{(2a)}(r_i) \approx \Delta r\,\sigma_e(r_i) \quad (3.13)$$

$$+ \Delta r\sum_{j=1}^{i-1}\sigma_e(r_j)\left[1 - \left(1 + \frac{i - 1/2}{i - j}\frac{\alpha}{\vartheta_w(\lambda, r_j)}\right)\right.$$

$$\left.\exp\left(-\frac{i - 1/2}{i - j}\frac{\alpha}{\vartheta_w(\lambda, r_j)}\right)\right]$$

for $i = 2, \ldots, n$. Eq. (3.13) is used for the evaluation of Eq. (2.8). To calculate the extinction coefficient $\sigma_e(r_i)$ in the first term of this equation start with the approximate value of Eq. (2.8) with $Q_{ms}^{(2a)}(r_i) = 0$.

4 The Exact Stochastic Model

The exact stochastic model (see Oppel et al., 1989; Noormohammadian, 1996) starts from a description of the process of multiple scattering deriving an exact lidar equation for the multiply scattered lidar return signal. Contrary to approximating methods for the calculation of the lidar return signal (see e.g. Bissonnette et al. (1995) and the previous sections of this article) a Monte Carlo simulation is used to calculate the exact lidar return signal.

The main drawback of the "physical" Monte Carlo method, i.e. simulating the physical scattering process, is often a too expensive cost for calculations with desired accuracy. This can be avoided by concentrating on the significant aspects of the given problem, leading to a reduction of the statistical variance for the same amount of computer time, i.e. increasing the efficiency of the computational scheme (see e.g. Spanier and Gelbard, 1969; Kalos and Whitlock, 1986; Bratley and Schrage, 1987).

On the basis of the stochastic model such variance reducing Monte Carlo methods like the local method (i.e. using the point flux estimator), the exponential transformation with splitting, and the "scattering splitting" were applied and developed. Using these methods, the Monte Carlo program enables the user to calculate the exact lidar return signal including all scattering orders for various environmental situations. The Monte Carlo program was verified by comparisons conducted around the MUSCLE workshop (see Bissonnette et al., 1995).

Comparing with the Monte Carlo program, the single and double scattering part of the lidar return signal approximated with the program based on the Formulas (2.4) and (3.3) was verified. This comparison showed a perfect agreement for the cirrus cloud situations described in Section 5. Furthermore, these calculations with the Monte Carlo program including all scattering orders show that especially for the cirrus cloud situations of Section 5 only the single and the double scattering part of the lidar return signal must be taken into account. These results verify the assumptions of Section 3 used for the design of the new inversion algorithm. The exact description of the

stochastic model, the code of the Monte Carlo program, and the data of this comparison may be found in Noormohammadian (1996).

Because of the fact that all scattering orders are taken into account and that the assumptions of Section 3 were not used, it is obvious that the Monte Carlo program needs more computing time than the program on the basis of the approximate Formulas (2.4) and (3.3).

5 Examples

5.1 Lidar Systems, Clouds, and Phase Functions

Typical lidar systems are using receiver field of view (FOV) angles α (half apertures) between ± 0.3 mrad and ± 1.5 mrad. The distance where a complete crossover of the receiver field of view and the laser beam takes place depends on the optical design. The reference distance r_0 (see Eq. (2.6)) which lays beyond the minimum distance is set to 1000 m.

Between 6 km altitude and the tropopause cirrus clouds are frequently present (see, e.g. Liou, 1992). For the calculations we assume cloud layers of 0.5 km vertical extension and optical depths of 0.1, 0.3, or 1.0 in the altitude range from $(6.6 \cdots 7.1)$ km or $(10.0 \cdots 10.5)$ km. For simplicity the extinction coefficient is taken to be constant within the cloud. It should be emphasised that any layering can be taken into account. Due to the low temperature at 10 km altitude the high level cloud is containing pure ice crystals, the lower level cloud may contain supercooled water droplets or ice crystals or a mixture of both.

For simplification the extinction coefficient σ_e is set to 0.0107 km^{-1} above and below the cloud, and a Rayleigh phase function is assumed. In comparison to a realistic hazy atmosphere (e.g. Jursa, 1985) this has no major effect on the results.

Phase functions of ice clouds were calculated by Hess and Wiegner (1991 and 1994) using particle distributions given by Heymsfield and Platt (1984); they were so kind to provide them to us. Table 1 gives an overview, containing the forward scattering phase functions $\beta'_{\lambda_0}(0, r_p)$ at scattering angle $\vartheta = 0$, the $1/e$-widths $\vartheta_w(\lambda_0, r_p)$ resulting from Eq. (3.10) and the lidar ratios σ_e/β depending on λ_0 and r_p. In clouds with absorption parts $\sigma_a/\sigma_e = 0$ the lidar ratios are equal to the reciprocal values of the backscatter phase function $\beta'_{\lambda_0}(\pi, r_p)$. The values of β' for $\vartheta = 0$ are reaching a value of 97400, which is up to 10^6

Table 1: Parameters of phase functions at wavelength $\lambda_o = 532$ nm of different ice crystal clouds at air temperatures θ, from Hess and Wiegner (1991 and 1994).

No.	θ °C	β'_{λ_0}	ϑ_w mrad	(σ_e/β)
1.1	$-(20\cdots25)$	95800	0.911	1.290
1.2	$-(25\cdots30)$	80400	0.995	1.276
1.3	$-(30\cdots35)$	97400	0.904	1.339
1.4	$-(35\cdots40)$	58100	1.170	1.224
1.5	$-(40\cdots45)$	36000	1.487	1.127
1.6	$-(45\cdots50)$	41700	1.381	1.142
1.7	$-(50\cdots55)$	12400	2.533	1.064
1.8	$-(55\cdots60)$	34700	1.514	1.124

Table 2: Parameters of phase functions at different wavelengths λ_0 of an ice crystal cloud at air temperature $\theta = -(55\cdots60)$ °C, including particles with less than 10 μm diameter, from Strauss and Wendling (1992) and Strauss (1994). (No. 3.1 and 3.2 describe Deirmendjian-C1 water droplet clouds.)

No.	λ_0 nm	β'_{λ_0}	ϑ_w mrad	σ_e/β
2.1	423	14500	2.343	0.877
2.2	550	8550	3.051	1.028
2.3	635	6580	3.478	1.048
2.4	780	4360	4.272	1.272
2.5	830	3850	4.546	1.120
2.6	1015	2560	5.575	1.359
2.7	1615	1020	8.833	1.709
2.8	3700	225	18.81	0.709
3.1	550	210.2	19.46	20.32
3.2	1100	60.5	36.27	20.00

times higher than those for an isotropic phase function. They are substantially higher than values given by Wendling (1979) for different particle size distributions and much higher than those of a Deirmendjian C1 type cloud (see Table 2, nos. 3.1 and 3.2). The resulting lidar ratios are smaller than the earlier mentioned and often used value of 14, but they keep within the values calculated by Macke (1993). This might be explained by a smaller reflection factor for clustered crystals than for single crystals. Contrary, the diffraction of radiation, passing particle clusters, according to the Babinet theorem is mainly depending on the size of clusters. Thus the extremely big values of forward scattering caused by diffraction ought to be realistic.

It should be mentioned, that the size distributions by Heymsfield and Platt do not contain particles smaller than 10 μm, due to the applied measurement technique. If there are still smaller particles present, they are reducing the phase function for small angles (forward scattering) following Eq. (3.4) in the same way as they have effect on the scattering coefficient $\sigma_s(r)$. During the CIRRUS'92 campaign (Strauss and Wendling, 1992) particle size distributions within cirrus clouds down to particle diameters of less than 10 μm were measured. Strauss (1994) analysed these data and kindly made them available to us. Table 2 gives an overview similar to Table 1, but the varying parameter is the wavelength instead of the temperature. In fact, the adding of small particles is reducing the forward scattering by a factor of 1/4 to 1/3. The wavelength dependence of the 1/e-width ϑ_w follows Eq. (3.10) quite well. The lidar ratios of the ice crystal clouds are similar to the numbers given in Table 1.

For the atmosphere below and above the cloud also the 1/e-widths ϑ_w are used which were derived from the forward scattering coefficients β'_{λ_0} by means of

Eq. (3.10), although the assumptions for the calculation are less adequate. The introduced error is acceptable and the contributions to the final result are small. The Rayleigh value used throughout this paper is $\vartheta_w = 816$ mrad.

To test the algorithm a simplified phase function was used. This test phase function has the following values:

$$\beta'(\vartheta,r) = \begin{cases} 0.318 \cdot 10^6 & \\ \quad \text{for } 0 \leq \vartheta \leq 1 \text{ mrad} & \\ 0.0 & \\ \quad \text{for } 1 \text{ mrad} < \vartheta < \pi - 1 \text{ mrad} & \\ 0.318 \cdot 10^{-3} & \\ \quad \text{for } \pi - 1 \text{ mrad} \leq \vartheta \leq \pi. \end{cases} \quad (5.1)$$

With this assumption nearly 100 % of the scattered radiation remains within a narrow cone around the primary beam. Hence, the forward scattering peak of the test phase function is by a factor of 2 larger than that of natural (large) aerosol particles, where the diffraction lobe contributes 50 % to the extinction coefficient (see text following Eq. (3.9)).

For the cloud at a height of 6.6 to 7.1 km we assume temperatures between $-(25\cdots30)$ °C. The phase function for the frequency doubled Nd:YAG wavelength 532 nm should remain between the extremely different types No. 1.1 (Table 1) and No. 3.1 (Table 2). These two phase functions are plotted in Figure 1. It can be seen clearly that the approximations following Eq. (3.9) are reasonable for these critical small scattering angles.
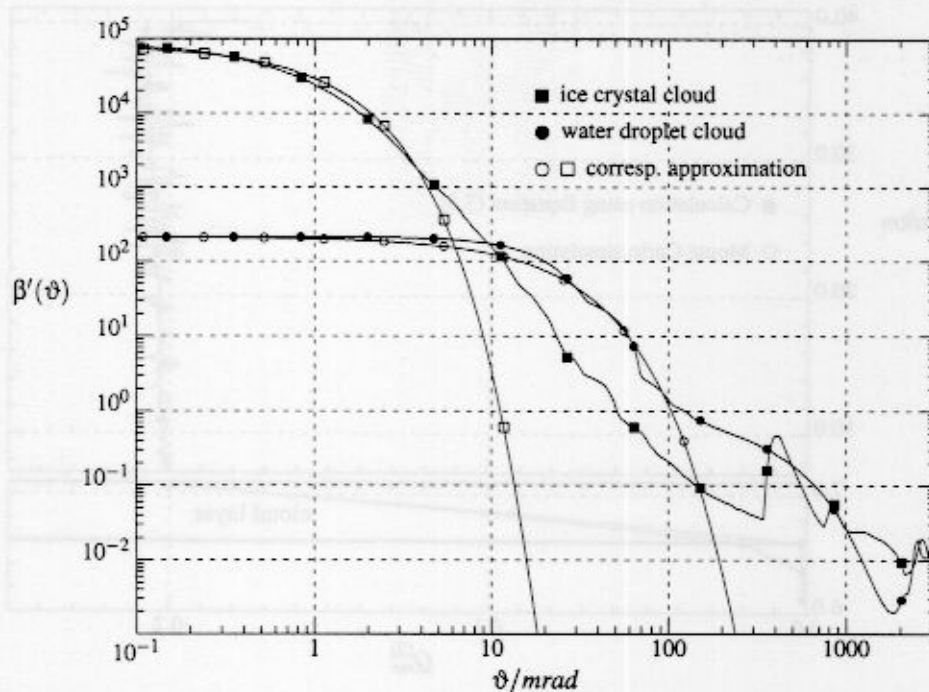
Figure 1: Phase functions for the clouds at the height of 6.6 to 7.1 km with temperature in the range $-(25\cdots30)$ °C. Filled squares: ice crystal cloud according to No. 1.1 of Table 1. Filled circles: water droplet cloud according to No. 3.1 of Table 2. Open symbols: approximations according to Eqs. (3.9) and (3.10).
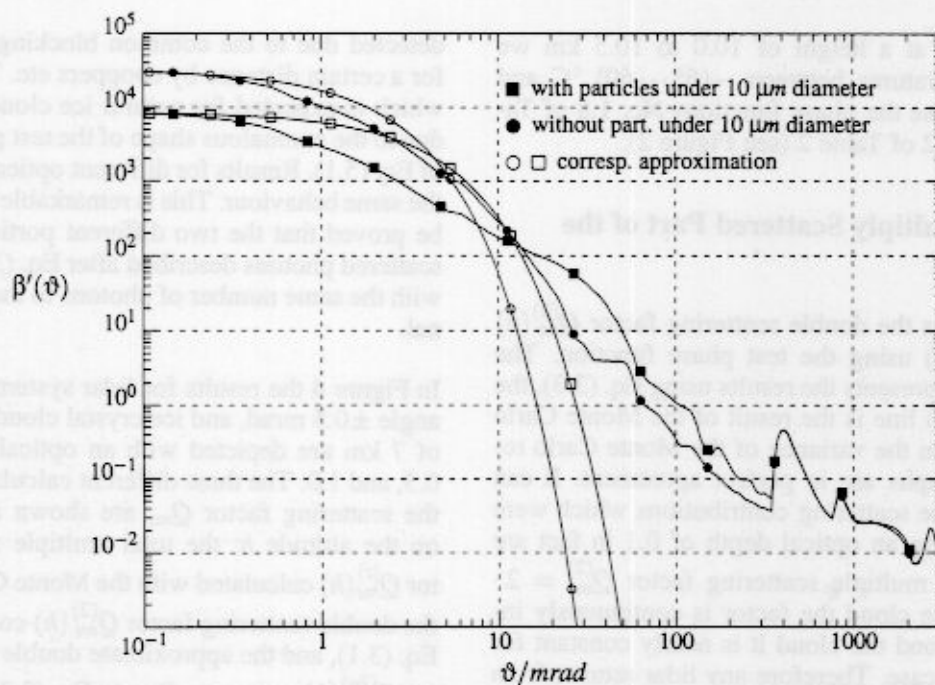

Figure 2: Phase functions for the clouds at the height of 10.0 to 10.5 km with temperature in the range $-(55\cdots60)$ °C. Filled circles: ice crystal cloud without particles under 10 μm diameter according to No. 1.8 of Table 1. Filled squares: ice crystal cloud with particles under 10 μm diameter according to No. 2.2 of Table 2. Open symbols: approximations according to Eqs. (3.9) and (3.10).
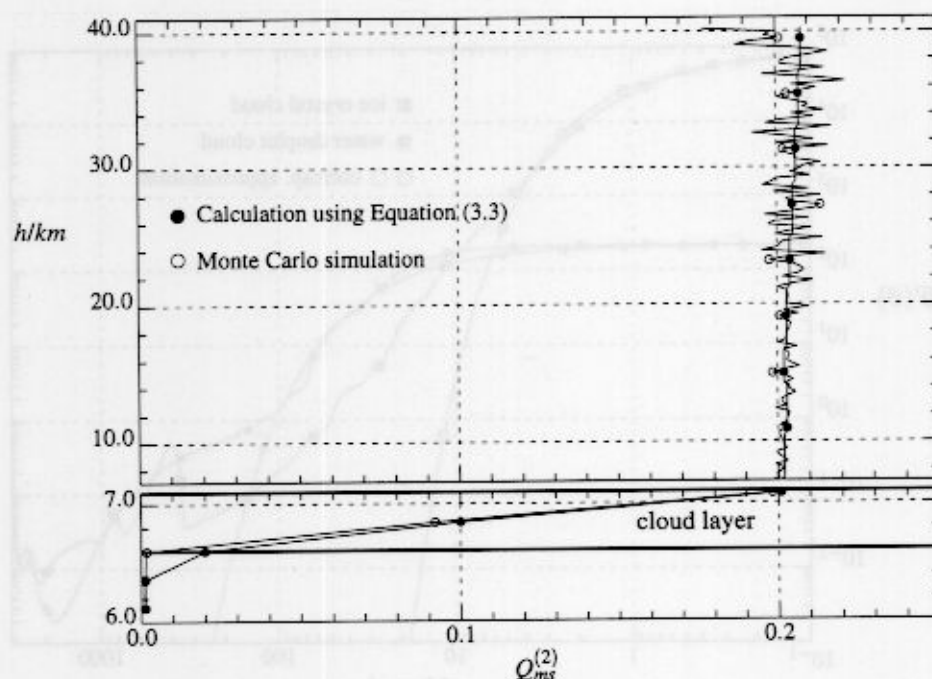
Figure 3: Double scattering factor $Q_{ms}^{(2)}(h)$ of Eq. (3.1) as a function of the height h for the 7 km cloud with the optical depth 0.1, the idealized test phase function, and a receiver *FOV* angle $\alpha = \pm 3$ mrad. Filled circles: results of the program according to Eq. (3.3). Open circles: results of the Monte Carlo program (see Section 4). The lower plot is enhancing the region within the cloud.

For the cloud at a height of 10.0 to 10.5 km we assume temperatures between $-(55 \cdots 60)$ °C and therefore we use the phase functions No. 1.8 of Table 1 or No. 2.2 of Table 2 (see Figure 2).

5.2 The Multiply Scattered Part of the Signal

Figure 3 shows the double scattering factor $Q_{ms}^{(2)}(h)$ from Eq. (3.1) using the test phase function. The smooth line represents the results using Eq. (3.3), the noisy (zig-zag) line is the result of the Monte Carlo method. Within the variance of the Monte Carlo results these graphs are in perfect agreement. It can be seen that the scattering contributions which were integrated along an optical depth of 0.1 in fact are resulting in a multiple scattering factor $Q_{ms}^{(2)} = 2 \cdot 0.1$. Within the cloud the factor is continuously increasing. Beyond the cloud it is nearly constant for this idealised case. Therefore any lidar returns from beyond the optically thin cloud are affected. The source of contradictions in lidar soundings from Polar Stratospheric Clouds, stratospheric temperature or densities might sometimes be found in an optically thin cloud in the troposphere, which was not

detected due to the common blocking of the signal for a certain distance by choppers etc. The value 0.1, which is expected for natural ice clouds, is doubled due to the anomalous shape of the test phase function of Eq. (5.1). Results for different optical depths show the same behaviour. This is remarkable because it can be proved that the two different portions of doubly scattered photons described after Eq. (3.2) contribute with the same number of photons to the received signal.

In Figure 4 the results for lidar systems with a *FOV* angle ± 0.5 mrad, and ice crystal clouds at the height of 7 km are depicted with an optical depth of 0.1, 0.3, and 1.0. The three different calculated values for the scattering factor Q_{ms} are shown in dependence on the altitude h: the total multiple scattering factor $Q_{ms}^{(t)}(h)$ calculated with the Monte Carlo program, the double scattering factor $Q_{ms}^{(2)}(h)$ corresponding to Eq. (3.1), and the approximate double scattering factor $Q_{ms}^{(2a)}(h)$ corresponding to Eq. (3.3). At the upper boundary of the cloud $Q_{ms}^{(2)}(h)$ is approaching the theoretical maximum value which is equal to the optical depth of the cloud being penetrated by the laser light. Thus, if multiple scattering is neglected in Eq. (2.8),
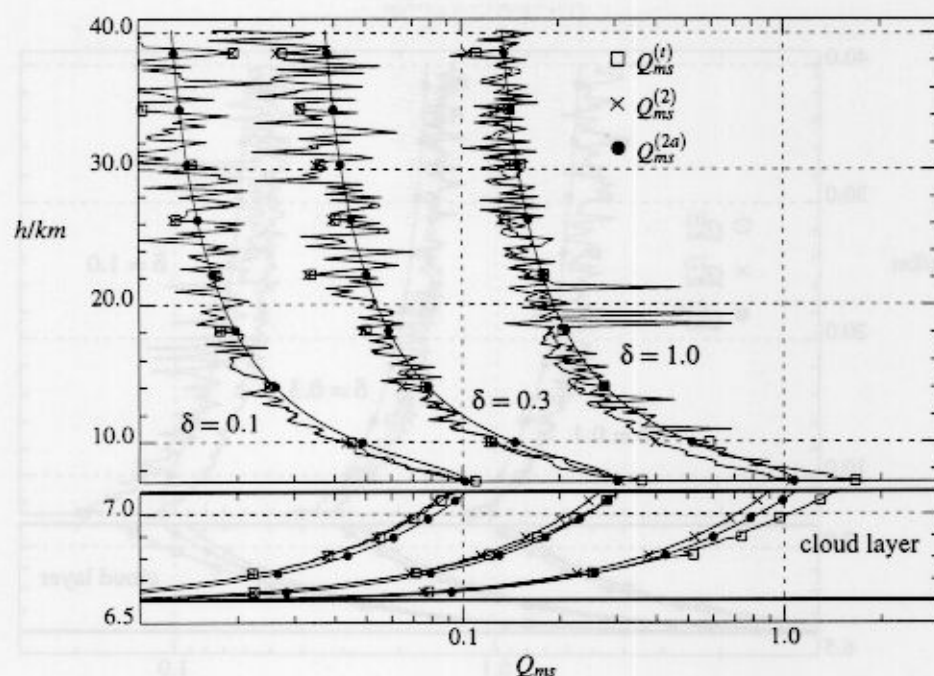
Figure 4: Q_{ms}-approximations as a function of the height h for ice crystal clouds at the height of 7 km with optical depths 0.1, 0.3 and 1.0 (left, middle and right group of curves) using lidar systems with a receiver FOV angle $\alpha = \pm 0.5$ mrad. Open Square: total multiple scattering factor $Q_{ms}^{(t)}(h)$ calculated with the Monte Carlo program. Crosses: double scattering factor $Q_{ms}^{(2)}(h)$ with respect to Eq. (3.1). Filled circles: approximated double scattering factor $Q_{ms}^{(2a)}(h)$ with respect to Eq. (3.13).

the extinction coefficient retrieved from the lidar signal are too large by 10 %, 30 %, and 100 %, respectively, not considering the overestimated transmission of the layer which was passed earlier by the laser light. For ground based systems there is even a distinct multiple scattering effect on return signals from 40 km altitude, having penetrated cirrus clouds at lower levels. This results in a deviation from the $1/r^2$ dependence.

The influence of remote ice crystal clouds which were passed by the radiation is more effective for the larger receiver FOV angle ± 1.5 mrad (see Figure 5). The values of $Q_{ms}^{(2)}(h)$ and $Q_{ms}^{(2a)}(h)$ in Figure 4 and Figure 5 are proportional to the optical depth of the corresponding cloud. The reason can be found in the fact that the cloud stratification $\sigma_s(r_p)$ in Eq. (3.11) in both figures are sufficiently similar. The stratifications would be exactly "similar" if $\sigma_s(r_p)$ in haze, too, would be proportional to the three different optical depths of the cloud. But the scattering coefficient for this haze model is so small that multiple scattering can be neglected. Going to smaller optical depths $Q_{ms}^{(t)}(h)$ and $Q_{ms}^{(2)}(h)$ are approaching. For

optical depths ≥ 1.0 the difference is becoming obvious. The approximation $Q_{ms}^{(2a)}(h)$ has the tendency to slightly higher values than those of $Q_{ms}^{(2)}(h)$ and $Q_{ms}^{(t)}(h)$ for small optical depths and reaches $Q_{ms}^{(t)}(h)$ at an optical depth around 1.0. The effect of double scattering in the far field is being overestimated due to the chosen simplified phase functions.

Figure 6 shows the situation for clouds, composed of water droplets, with an optical depth of 1.0 and for two different FOV angles ($\alpha = \pm 0.5$ mrad / $\alpha = \pm 1.5$ mrad). For both assumptions the maxima of $Q_{ms}^{(2)}(h)$ and $Q_{ms}^{(2a)}(h)$ remain below the theoretical maximum (equal to the optical depth of the cloud being observed). Only for the wider FOV this value is nearly achieved at the upper boundary of the cloud. The phase function for the C1 water cloud is less steep than that for ice crystal clouds. Therefore the contributions $Q_{ms}(h)$ are rapidly dropping beyond the cloud.

For a cloud at higher altitude the results are similar to the ice crystal cloud shown in Figure 4. Also the changes in shape of the phase functions No. 1.8 and
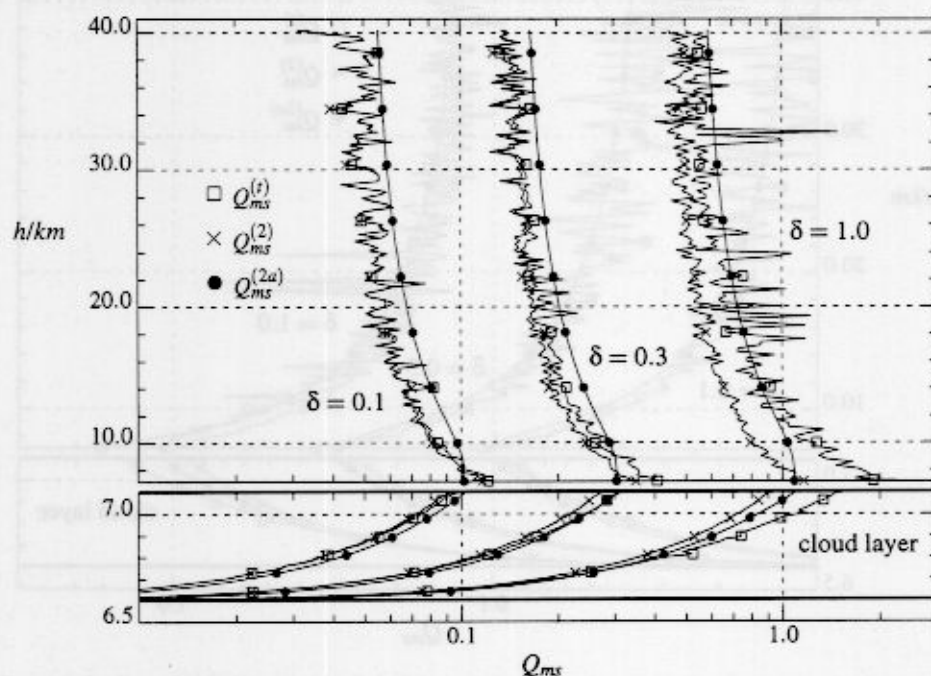
Figure 5: Same as Figure 4, showing the Q_{ms}-approximations as a function of the height h ice crystal clouds at the height of 7 km using lidar systems with a receiver *FOV* angle $\alpha = \pm1.5$ mrad.
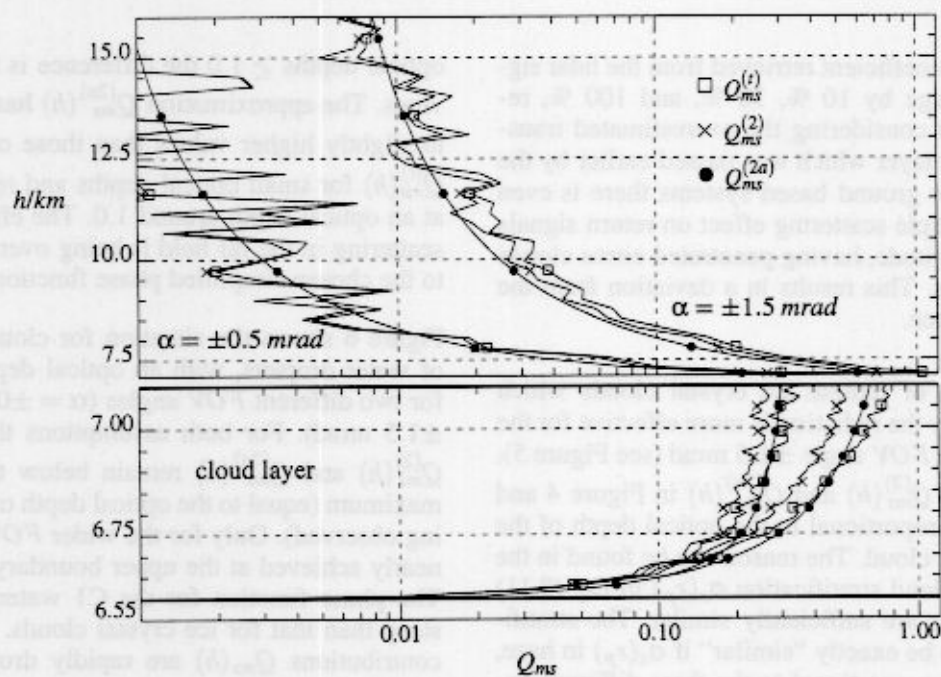

Figure 6: Same as Figure 4, showing the Q_{ms}-approximations as a function of the height h for water droplet clouds at the height of 7 km with the optical depth 1.0 using lidar systems with a receiver *FOV* angle $\alpha = \pm0.5$ mrad (left group of curves) and $\alpha = \pm1.5$ mrad (right group of curves).

2.2, which are expected to be adequate at higher altitude, are insignificant compared to those at 7 km altitude where clouds composed of ice crystals and super-cooled water droplets have to be taken into account.

5.3   Inversion of the Lidar Signal from the Cirrus

By application of the variance reduction Monte-Carlo Method (see Section 4), regarding any order of scattering, the multiple scattering factors $Q_{ms}^{(t)}$ ($\equiv Q_{ms}$) were calculated for different cloud models and their corresponding phase functions as well as the different lidar configurations, mentioned in Section 5.1. Thus a number of simulated lidar profiles could be established.

Using these artificial profiles by applying Eq. (2.8) during consecutive iterations, profiles of the extinction coefficient and of the optical depth could be retrieved. Besides others the multiple scattering approximation following Eq. (3.13) was used for the inversion. One general problem is, that the phase function for the observed cloud is not well known. The possible errors resulting from different phase functions have been investigated and are shown in Figures 7 to 12. These calculations were performed only for the narrow FOV systems ± 0.5 mrad and the cloud at 7 km altitude.

Figures 7 to 12 show the inverted extinction coefficient $\sigma_e^{(inv)}(h)$ and the inverted optical depth $\delta^{(inv)}(0,h)$ each of them normalised to the known values of the model assumption in dependence on the range which is consistent with the altitude h. For the cloud model in Figures 7 to 9, a Deirmendjian type C1 cloud, containing super-cooled water droplets, was taken into account (No. 3.1 in Table 2). For Figures 10 to 12 this cloud model was replaced by the ice crystal cloud No. 1.1 (Table 1). The different multiple scattering factors described in Table 3 are used.

The graphs in Figure 7 were calculated for an optical depth of 0.1. The Graphs 1 to 3 show only very small deviations from the original (model) assumptions. For Graph 4 and 5 the deviation becomes obvious within the cloud and for ca. 2 km beyond.

The reason that in the examples all inverted extinction coefficients are systematically too high by 2% and the optical depths by 4% can be found in the relatively large integration steps of 240 m which were taken below and above the cloud to reduce the computing time.

For the cloud model with an optical depth of 0.3 in Figure 8 the inversion using just double scattering (Graph 2) is giving nearly the same result as the algorithm regarding all scattering orders. Also the double scattering approximation using the right phase function is sufficient. The assumption of a wrong phase function (Graph 4) in this case an ice crystal phase function leads to slightly higher deviations (-22 %) of the extinction coefficient than the skipping of the multiple scattering effect in Graph 5 (+20 %) while the calculation of the optical depth leads to an even smaller relative error for the wrong phase function. (8 % compared to 9 %).

In Figure 9 results from more dense clouds are depicted. The errors are dramatically increasing if multiple scattering is not taken into account. Close to the upper boundary of the cloud the extinction coefficient is "exploding" the optical depth is even rapidly increasing beyond the cloud and reaching meaningless high values. The approximation using the wrong phase function is producing extinction coefficients which are too small but the error for the optical depth is kept within acceptable 25 %. For an optical depth of 1.0 also the deviations between Graphs 1, 2, and 3 become non negligible. In this particular case the inversion using $Q_{ms}^{(2a+)}$ is even better than the inversion using $Q_{ms}^{(2)}$, resulting from the approximation of the phase function according to Eq. 3.9. In order to avoid the instability showing up in Graph 5, it is also possible to change the lidar ratio incrementally until the extinction coefficient beyond the cloud is approaching values which are known or may be estimated (see e.g. Renger et al., 1995; Schreiber et al., 1995). But one should be aware that in this case errors due to neglecting of multiple scattering are corrected by the assumption of wrong lidar ratios.

Also for ice crystal clouds (Figures 10 to 12) the approximation method is producing adequate results up to an optical depth of 1.0 if the correct phase function is known. Using an extremely wrong phase function (here a C1 cloud) the results are reasonable up to an optical depth of 0.3. For all examples the application of the approximation method even using a wrong phase function is giving less erroneous results than a classical inversion not regarding multiple scattering. This can be explained by the following considerations:

The approximation method is correctly taking into account the double scattering contribution $Q_{ms}^{(2)}$ at the actual range step, because the factor $Q_{ms}^{(2)}$ is mainly independent from the phase function at distance r_i (see Eq. (3.13). Even in optically thin clouds $Q_{ms}^{(2)}$
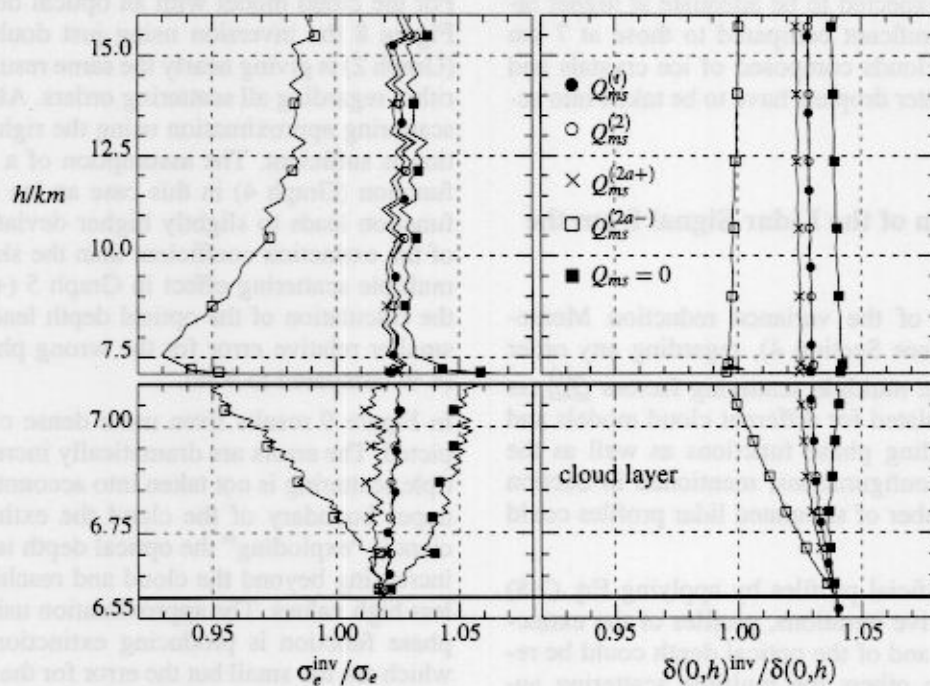
Figure 7: Ratio of the extinction coefficient $\sigma_e^{(inv)}(h)$ to the given values $\sigma_e(h)$ (left plot), and ratio of the optical depth $\delta^{(inv)}(0,h)$ to the given values $\delta(0,h)$ (right plot) as a function of the height h. The inverted signals were simulated using a 7 km cloud with the optical depth 0.1, and the C1 water droplet phase function No. 3.1 of Table 2. Within the signal inversion the assumptions concerning the multiple scattering factor Q_{ms} described in Table 3 were made. The lower parts of the plots are enhancing the region within the cloud.
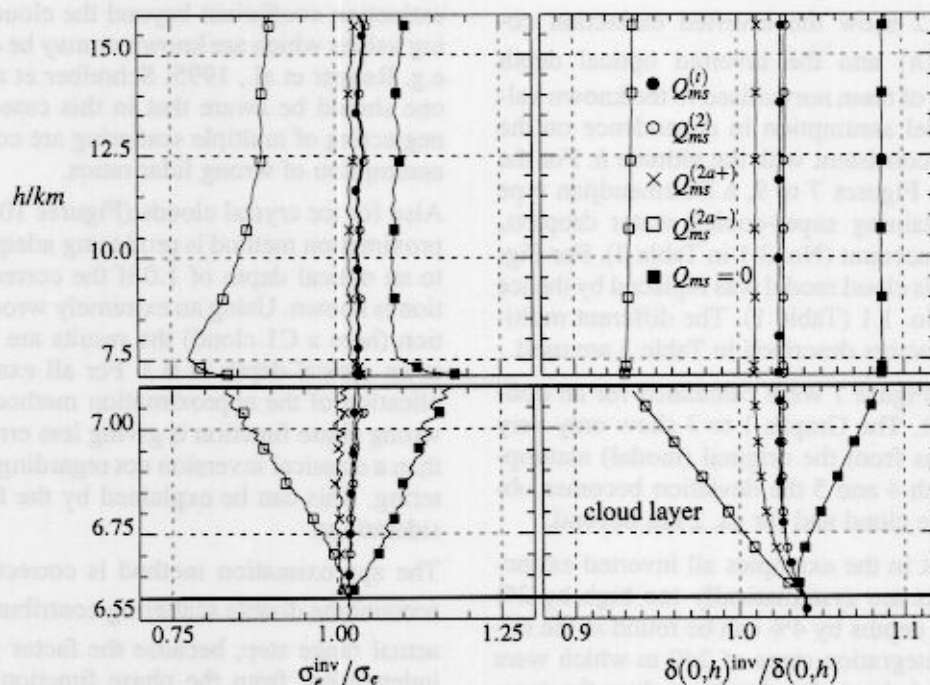

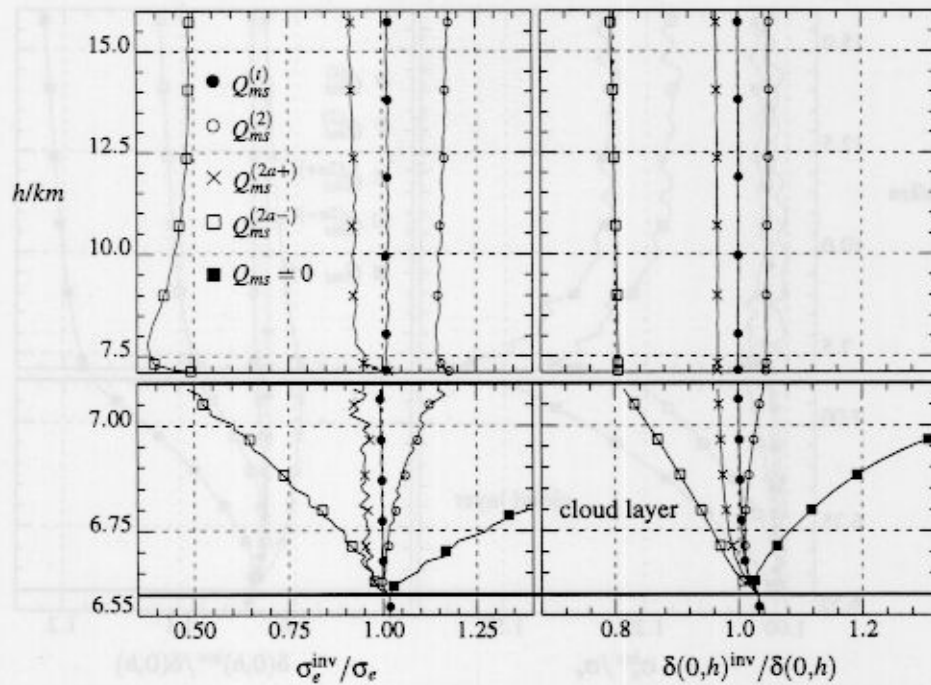**Figure 8:** Same as Figure 7 with a water droplet cloud at the height of 7 km but an optical depth 0.3 was used.

Figure 9: Same as Figure 7 with a water droplet cloud at the height of 7 km but an optical depth 1.0 was used.
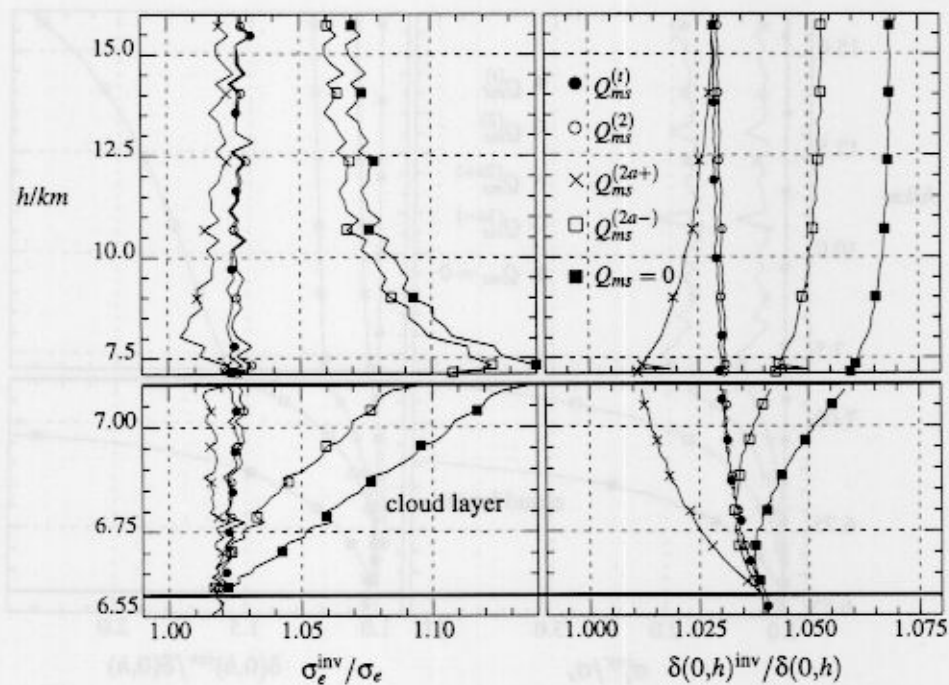

Figure 10: Same as Figure 7, except that the inverted signals were simulated using an ice crystal cloud with phase function No. 1.1 of Table 1 at the height of 7 km with an optical depth 0.1.

Figure 11: Same as Figure 7, except that the inverted signals were simulated using an ice crystal cloud with phase function No. 1.1 of Table 1 at the height of 7 km with an optical depth 0.3.
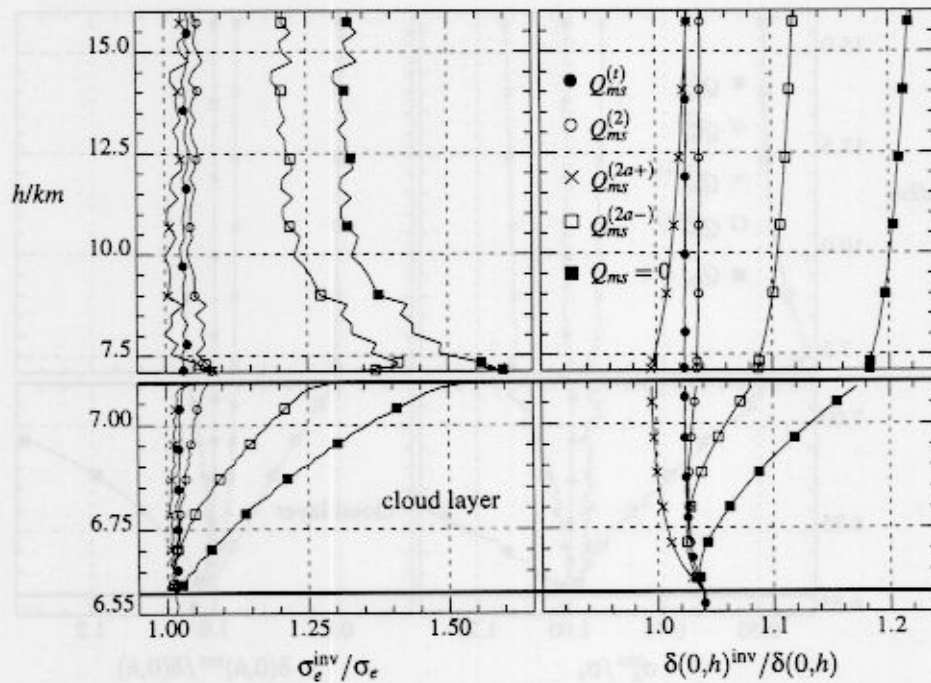

Figure 12: Same as Figure 7, except that the inverted signals were simulated using an ice crystal cloud with phase function No. 1.1 of Table 1 at the height of 7 km with an optical depth 1.0.
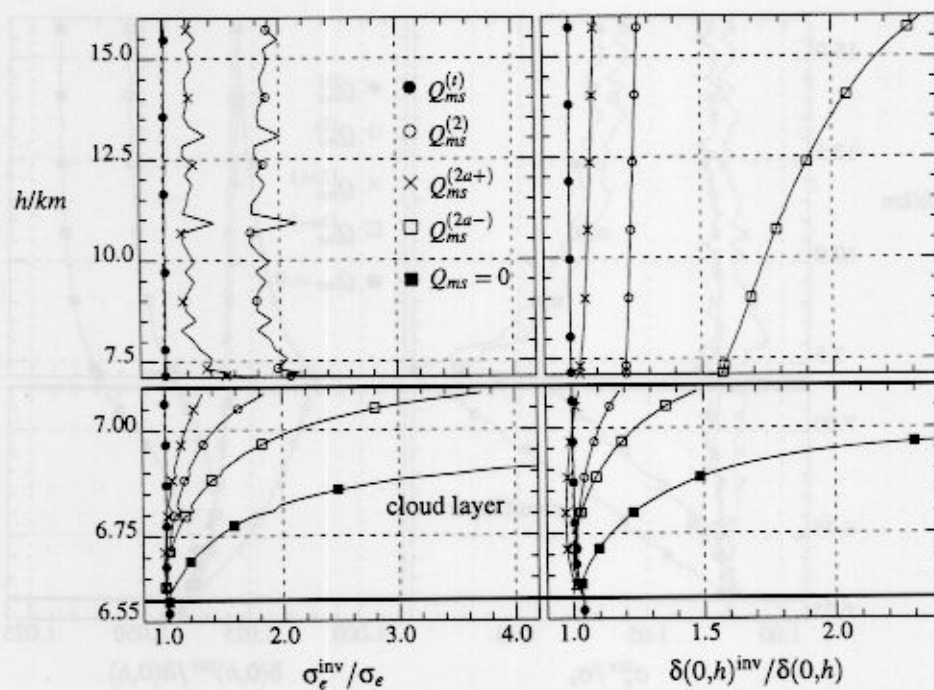
Table 3: Different assumptions made for the multiple scattering term.

Nos.		Description	Graph with ...
1	$Q_{ms}^{(t)}$	All scattering orders included.	filled circles
2	$Q_{ms}^{(2)}$	Single and double scattering is being regarded.	open circles
3	$Q_{ms}^{(2a+)}$	Double scattering approximation is used with the correct phase function known from the model.	crosses
4	$Q_{ms}^{(2a-)}$	Double scattering approximation is used with the phase function of the wrong cloud type.	open squares
5	$Q_{ms} = 0$	Multiple scattering being neglected.	filled squares

is significantly differing from zero. The assumption $Q_{ms} = Q_{ms}^{(2)} = 0$ is resulting in an overestimation of the extinction coefficient $\sigma_e(r_i)$ (see Eq. (2.8)). The consequence is that for the next sample intervals the transmittance $\tau(r_{i+k})$ is being underestimated resulting in further enlarged extinction coefficients $\sigma_e(r_{i+k})$. For the consecutive samples repetitive effect this makes the extinction coefficient to follow an exponential law of the range which was formerly called "explosion" of the inversion.

In contrast, when applying the approximation method non negligible errors arise at range intervals beyond the cloud only if wrong phase functions are introduced. E.g. in Figure 11 a phase function is used which is too flat. This means that an essential part of the scattered radiation is leaving the FOV earlier, thus reducing the probability that a second scattering process takes place within the FOV. $Q_{ms}^{(2)}$ is being underestimated leading to an overestimation of $\sigma_e(r_{i+k})$. Eq. (3.13) is raising $Q_{ms}^{(2)}$ and this opposite effect is effectively reducing errors produced by an inadequate phase function.

6 Conclusions

Ice crystals of natural clouds scatter about 50 % of the primary scattered radiation in a very small cone around the primary beam. This part of the scattered radiation stays therefore over long distances within the field of view of a lidar, and is contributing to the primary irradiation. This portion, and the resulting contribution from further scattering processes, which is part of the multiply scattered lidar return signal, are taken into account in the lidar equation by the factor $(1 + Q_{ms}(r))$. The multiple scattering factor $Q_{ms}(r)$ describes the ratio of the multiple to the single scattering lidar return signal.

Monte Carlo simulations on the basis of the exact stochastic model show for ground-based lidar measurements up to optical depths of about 1.0 that higher scattering orders than double scattering may be neglected. Thus the double scattering factor $Q_{ms}^{(2)}(r)$ is a good approximation for the multiple scattering factor $Q_{ms}(r)$, except for long range lidar applications. $Q_{ms}^{(2)}(r)$ changes its value proportional to the ratio of the FOV to the width of the forward scattering lobe and covers values from zero to the optical depth between the lidar and the distance r. Neglecting multiple scattering the inversion of a lidar signal will result in overestimating the extinction coefficients and optical depths for increasing distance r. Taking into account error-increasing effects, neglecting multiple scattering may lead to an explosion of the inversion procedure. Using further information such an explosion can be avoided deceiving too small lidar ratios $(\sigma_e/\beta)(r)$, where the errors of the resulting $(\sigma_e/\beta)(r)$ are increasing with the optical depth.

The double scattering factor $Q_{ms}^{(2)}(r)$ may be calculated within the inversion of the lidar signal with a very simple and extremely fast approximation. Besides the FOV angle only the $1/e$-width $\vartheta_w(\lambda,r)$ of the approximated phase function is required. For wavelength $\lambda = 532$ nm the $1/e$-widths for ice crystal clouds are in a range of $\vartheta_w(\lambda,r) = (0.9 \cdots 3.0)$ mrad, for water droplet clouds $\vartheta_w(\lambda,r) \approx 19$ mrad must be used. Even wrong values of $\vartheta_w(\lambda,r)$ have small effects on the inverted extinction coefficients and optical depths. This is due to the stability of the presented inversion algorithm using the double scattering approximation. The inversion is even acceptable if, e.g., signals from an undercooled water droplet cloud ($\vartheta_w(\lambda,r) \approx 19$ mrad) will be inverted with the $\vartheta_w(\lambda,r) = 0.9$ mrad of an ice crystal cloud, or vice versa.

The proposed inversion algorithm using an approximation of the doubly scattered part of the lidar return signal is a stable and very fast inversion algorithm for the described meteorological situations.

References

Ansmann, A.; Wandinger, U.; Riebesell, M. and Weitkamp, C.; 1992: Independent measurement of extinction and backscatter profiles in cirrus clouds by using a combined Raman elastic-backscatter lidar. Appl. Opt. **31**, 7113–7131.

Blaettner, W.G.; Collins, D.G. and Wells, M.B.; 1974: The effects of multiple scattering on backscatter lidar measurements in fogs. Radiation Research Associates, Inc., prepared for Air Force Cambridge Res. Labs., 85 pp., Distributed by NTIS (National Technical Information Service), U.S. Dept. of Commerce, 5285 Port Royal Road, Springfield Va. 22151.

Bissonnette, L.R.; Bruscaglioni, P.; Ismaelli, A.; Zaccanti, G.; Cohen, A.; Benayahu, Y.; Kleiman, M.; Egert, S.; Flesia, C.; Schwendimann, P.; Oppel, U.G.; Starkov, A.V.; Noormohammadian, M.; Winker, D.M.; Zege, E.P.; Katsev, I.L. and Polonsky, I.N.; 1995: Lidar Multiple Scattering from Clouds. Appl. Phy. **B 60**, 4.

Bratley, P.; Fox, L.F. and Schrage, L.E.; 1987: A Guide to Simulation. Springer, New York.

Carnuth, W. and Reiter, R.; 1986: Cloud extinction profile measurements by using Klett's inversion method. Appl. Opt. **25**, 2899–2907.

Dubinsky, R.H.; Carswell, A.I. and Pal, S.R.; 1985: Determination of cloud microphysical properties by laser backscattering and extinction measurements. Appl. Opt. **24**, 1614–1622.

Eloranta, E.W.; 1972: Calculation of doubly scattered lidar returns. Ph. D. thesis, University of Wisconsin, Madison, 115 pp.

Gratzki, A.; 1991: Bestimmung der vertikalen Verteilung des Eisgehaltes in Cirruswolken aus kombinierten Lidar und Infrarot-Radiometer Messungen. Inaugural-Dissertation zur Erlangung des Doktorgrades der Mathematisch-Naturwissenschaftlichen Fakultät der Universität Köln, 99 pp.

Hess, M. and Wiegner, M.; 1991: Optical properties of hexagonal ice crystals. Model calculations. Conf. Rept. ICO – Topical meeting on atmospheric, volume and surface scattering and propagation, Florence, Italy, Aug. 27–30.

Hess, M. and Wiegner, M.; 1994: COP: A data library of optical properties of hexagonal ice crystals. Appl. Opt. **33**, 7740–7746.

Heymsfield, A.J., Platt, C.M.R.; 1984: A parameterization of the particle size spectrum of ice clouds in terms of the ambient temperature and the ice water contend. J. Atmos. Sci. **41**, 846–855.

van de Hulst, H.C.; 1980: Multiple scattering, tables, formulas, and applications. Volume 2. Academic Press, New York.

Jursa, A.S. (ed.); 1985: Handbook of Geophysics and the Space Environment. Air Force Geophysics Laboratory, Air Force Systems Command, U.S. Air Force.

Kaestner, M.; Kriebel, K.T.; Meerkoetter, R.; Renger, W.; Ruppersberg, G.H and Wendling, P.; 1993: Comparison of cirrus height and optical depth derived from satellite and aircraft measurements. Mon. Wea. Rev. **121**, 2708–2717.

Kalos, M.H. and Whitlock, P.A.; 1986: Monte Carlo Methods, Vol. 1. Wiley, New York.

Klett, J.D.; 1980: On the analytical inversions of lidar returns from an inhomogeneous atmosphere. Contract DAADO7-79-C-0008, U.S. Army Electronics Res. and Dev. Command, Atm. Sc. Lab., White Sand Missiles Range, NM 88002.

Klett, J.D.; 1981: Stable analytical inversion solution for processing lidar returns. Appl. Opt. **20**, 211–220.

Klett, J.D.; 1985: Lidar inversions with variable backscatter/extinction ratios. Appl. Opt. **24**, 1638–1643.

Liou, K.N.; 1992: Radiation and cloud processes in the atmosphere. Oxford Monographs on Geology and Geophysics No. 20, Oxford University Press, Oxford.

Macke, A.; 1993: Scattering by polyhedral ice crystals. Appl. Opt. **32**, 2780–2788.

Moerl, P.; Reinhardt, M.E.; Renger, W. and Schellhase, R.; 1981: The use of the airborne LIDAR system "ALEX F 1" for aerosol tracing in the lower troposphere. Beitr. Phys. Atmosph. **54**, 401–410.

Muetze, K. (ed.); Foitzik, L.; Krug, W. and Schreiber, G.; 1961: ABC der Optik. VEB F.A. Brockhaus Verlag, Leipzig, 964pp.

Noormohammadian, M.; 1996: Varianzreduzierende Monte-Carlo Methoden zur Berechnung mehrfach gestreuter LIDAR Rücksignale. Dissertation zur Erlangung des Doktorgrades der Mathematischen Fakultät der Ludwig-Maximilians-Universität München, 323 pp.

Oppel, U.G.; Findling, A.; Krichbaumer, W.; Krieglmeier, S. and Noormohammadian, M.; 1989: A stochastic model for the calculation of multiply scattered LIDAR returns. DLR-Forschungsbericht, 89–36, Köln, 219pp.

Pinnick, R.G.; Jennings, S.G.; Chylek, P.; Ham, C. and Grandy jr., W.T.; 1983: Backscatter and extinction in water clouds. J. Geophys. Res. **88**, 6787–6796.

Platt, C.M.R.; 1973: Lidar and radiometric observation of Cirrus clouds, J. Atmos. Sci. **30**, 1191-1204.

Renger, W.; Wirth, M.; Schreiber, H.G.; Kiemle, C. and Moerl, P.; 1995: Correlative measurements in support of LITE. ELITE workshops, Florenz, 9.–10.11.1995, ESA WPP-107, 15–30.

Ruppersberg, G.H. and Renger, W.; 1990: Shadow technique for improved inversion of lidar data to cirrus and contrail optical depth. Proceedings of International Cirrus Experiment. Third workshop in Villeneuve d'Ascq, France, 3–5 Dec. 1990. Edited by G. Brogniez and F. Parol, Laberatoire d'Optique Atmospherique, Universite des Sciences et Techniques de Lille Flandres Artois.

Schmitz-Peiffer, A. and Renger, W.; 1991: Lidarverfahren. promet 1/2, 24–33.

Schreiber, H.G.; Moerl, P.; Wirth, M. and Renger, W.; 1995: Airborne backscatter Lidar measurements at 3 wavelengths during ELITE. European symposium on 'Optics for Environmental and Public Safety', München, 19.–23.6.1995. Proc. Europto Series, Vol. 2505, 55–65.

Spanier, J. and Gelbard, E.M.; 1969: Monte Carlo Principles and Neutron Transport Problems. Series in Computer Science and Information Processing. Addison-Wesley, Reading.

Strauss, B. and Wendling, P.; 1992: CIRRUS'92: Cirruswolkenexperiment Oktober 1992 Oberpfaffenhofen, Experimentplan. DLR – Institut für Physik der Atmosphäre, Oberpfaffenhofen, 18 pp.

Strauss, B.; 1994: Ueber den Einfluß natürlicher und anthropogener Eiswolken auf das regionale Klima – mit besonderer Berücksichtigung des mikrophysikalischen Einflusses. Dissertation der Fakultät für Physik der Ludwig-Maximilians-Universität München, 96 pp.

Wandinger, U.; 1996: Multiple-scattering influence on extinction- and backscatter coefficient measurements with Raman and high-spectral-resolution lidars. Subm. to Appl. Opt.

Weinman, J.A.; 1976: Effects of multiple scattering on light pulses reflected by turbid atmospheres. J. Atmos. Sci. **33**, 1763–1771.

Wendling., P.; Wendling., R. and Weickmann, H.K.; 1976: Scattering of solar radiation by hexagonal ice crystals. Appl. Opt. **18**, 2663–2671.

Werner, Ch.; Streicher, J.; Herrmann, H. and Dahn, H.G.; 1992: Multiple-scattering lidar experiments. Optical Engineering **31**, 1731–1744.